An Admittance-Controlled Robotic Assistant for Semi-Autonomous Breast Ultrasound Scanning

Jay Carriere[1], Jason Fong[1], Tyler Meyer[2], Ron Sloboda[3], Siraj Husain[2], Nawaid Usmani[3], and Mahdi Tavakoli[1]

***Abstract*— Ultrasound imaging has been shown to successfully diagnose and provide visual assistance during treatment of breast cancer. However, human operators (i.e., technicians and clinicians) provide limited repeatability when performing the imaging scans. Current state-of-the-art automated breast volume scanners (ABVS) have high repeatability but deform the breast tissue significantly, which is undesirable for percutaneous therapies such as brachytherapy. A semi-autonomous system is presented here which leverages the accuracy of a serial manipulator-design robotic assistant to maintain the ultrasound probe at an optimal angle and ensure stable contact with minimal tissue deformation. Positioning of the probe across the surface of the breast is left in the hands of the human operator and is enabled through an admittance controller for the robot. A feasibility study is performed through a comparison of imaging quality for ultrasound scans of a simulated seroma in a phantom tissue when performed with human-in-the-loop and fully-autonomous modalities. The system was evaluated in a user trial showing similar image quality performance to a fully-autonomous position-controlled scanning device.**

$\{B\}$	Robot Base Frame
$\{C\}$	3D Scanner Frame
$\{S\}$	Moving Surface Frame
${}^{B}\vec{P}$	Position Vector in Robot Base Frame
${}^{C}\vec{P}$	Position Vector in 3D Scanner Frame
${}^{S}\vec{P}$	Position Vector in Moving Surface Frame
${}^{B}\vec{V}$	Velocity Vector in Robot Base Frame
${}^{B}_{S}T$	Transformation from Surface Frame to Base Frame
${}^{S}_{B}T$	Transformation from Base Frame to Surface Frame

This research was supported by the Canada Foundation for Innovation (CFI) under grant LOF 28241; the Alberta Innovation and Advanced Education Ministry under Small Equipment Grant RCP-12-021; the Natural Sciences and Engineering Research Council (NSERC) of Canada under the Collaborative Health Research Projects (CHRP) Grant #316170; and the Quanser, Inc.

[1]Jay Carriere (Corresponding Author), Jason Fong, and Mahdi Tavakoli are with the Department of Electrical and Computer Engineering, University of Alberta, AB, Canada T6G 1H9. jtcarrie@ualberta.ca, jmfong@ualberta.ca, mahdi.tavakoli@ualberta.ca

[2]Tyler Meyer and Siraj Husain are with the Division of Radiation Oncology, Tom Baker Cancer Centre, 331 29th Street NW, Calgary, Alberta T2N 4N2. Tyler.Meyer@albertahealthservices.ca, siraj.husain@albertahealthservices.ca.

[3]Ron Sloboda and Nawaid Usmani are with the Department of Oncology, Cross Cancer Institute, 11560 University Avenue, Edmonton, AB, Canada, T6G 1Z2. nawaid.usmani@albertahealthservices.ca, ron.sloboda@albertahealthservices.ca.

978-1-5386-7825-1/19/$31.00 **©2019 IEEE**

I. INTRODUCTION

According to current statistics, 1 in 4 Canadian women will be diagnosed with breast cancer in their lifetimes, with breast cancer representing the third most commonly diagnosed cancer in the general population [1]. Ultrasound imaging has shown to be highly effective for diagnosing breast cancers [2], but has limited repeatability when performed by a technician or clinician. For imaging repeatability, the orientation of the ultrasound probe with respect to tissue should be the same every time the probe passes over a particular point on the surface of the tissue. In addition to diagnostic imaging, ultrasound can be used for interventional imaging during percutaneous (needle-based) therapies, such as breast permanent seed implant brachytherapy (BPSIB) and breast tissue biopsy. Such procedures have been shown to benefit from live ultrasound image feedback to increase needle-tip placement accuracy [3].

Several innovations exist to address the shortcomings of hand-held ultrasound imaging. Authors in [4] designed and validated a tracked mechanical arm that tracks the position of the ultrasound probe, but provides no actuated robotic assistance to the operator. On the other hand, automated breast volume scanners (ABVS) provide full automation of the scanning process [5]. However, existing ABVS devices, such as [6], purposely deform (compress) the breast during the ultrasound scan (similar in principle to the technique used for mammography), to enable scan repeatability and automatic volume creation. While this tissue compression in existing ABVS solutions allows for repeatable pre-clinical diagnostic imaging, it makes the ABVS techniques unsuitable for interventional imaging during percutaneous procedures. In particular, in the case of BPSIB, the current workflow involves first scanning the breast to create a treatment planning volume, planning the seed implantation locations and dosimetry based on this volume, and then performing the insertion using ultrasound image feedback [7], [8], [9], [10], [11]. This workflow relies on the breast remaining relatively undeformed during imaging and seed implantation.

In this work, we propose an ultrasound-scan assistant system which provides the benefits of an ABVS, namely repeatability and accurate position measurement, while keeping the surgeon in the loop by allowing the ultrasound technician or clinician to move the probe as required. In this system, a position controller is used such that the ultrasound probe holding assistant presses the probe to a desired depth below

the surface of the breast during the scan and orients the probe to conform to the surface shape. The controller is designed to minimize tissue compression during the scan while maximizing ultrasound image quality. An impedance-based controller allows for the user-directed movement of the robot (and probe). For physical human-robot interaction (PHRI) systems, impedance control strategies are often preferable to position control. Impedance control is an example of a basic force control strategy [12], [13]. Impedance controllers produce a desired force through a predefined relationship with the motion of the robot, which is typically converted to torque commands for the robot to carry out. However, this approach typically requires knowledge of the robot's dynamics and dynamics parameters, the latter of which are not made available for the robot used. In this work, we instead choose to use an admittance controller. Admittance controllers produce a desired motion through a predefined relationship with measured force [13], [14], [15]. Force-based controllers have seen successful application in assistive robotics-based medical devices, such as in upper limb robotic rehabilitation [16], [15] and in teleoperation-based imaging [17], [18].

The paper is organized as follows. Section II provides an explanation of the different frames of reference needed for imaging and robot control. Section III outlines the controller design that incorporates both human-in-the-loop input and autonomous robot control. The experimental setup and results for the feasibility study are presented in Section IV. Finally, concluding remarks and future directions are provided in Section V.

II. FRAME TRANSFORMATION AND SURFACE TRACKING

To implement the admittance controller, three different frames are used as shown in Fig. 1. The first frame is the base frame of the robot and is denoted by $\{B\}$. The surface (or contour) of the breast can be captured using a Kinect or other 3D scanner, and the second frame, $\{C\}$, is defined as the coordinate system used by the 3D scanning hardware. The 3D scanning hardware returns the points along the surface of the breast, ${}^{C}\vec{P}_c$. Given that the goal of the admittance controller is to minimize the force exerted by the ultrasound probe on the breast and thereby minimize breast deflection during the scan, in this work the forces are kept low such that we assume that the breast remains stationary during the scan. Under this assumption, the 3D scanner frame $\{C\}$ is registered to the robot base frame $\{B\}$ such that the surface contour points ${}^{C}\vec{P}_c$ are transformed into the robot base frame, where ${}^{B}\vec{P}_c = {}^{C}_{U}T\,{}^{C}\vec{P}_c$, before the ultrasound scan begins. After registration, the breast surface is represented topologically as a smooth 2D surface embedded in 3D space, such that the surface's z_c coordinate is dependant on its x-y coordinates, ${}^{B}z_c = f_c({}^{B}x, {}^{B}y)$, where the values returned by the function $f_c({}^{B}x, {}^{B}y)$ are empirically measured by the 3D scanner. For points in the ${}^{B}x - {}^{B}y$ plane (in the robot base frame) which are not on the surface of the breast, $\{{}^{B}x, {}^{B}y \notin C\}$, the surface function is clamped to some constant value, z_{min}, such that $f_c({}^{B}x, {}^{B}y) = z_{min} \forall \{{}^{B}x, {}^{B}y \notin C\}$, to define f_c within the entire workspace of the robot.

During ultrasound scanning, the scan assistant robot will be controlled such that the ultrasound probe can move freely along the surface of the breast, with the probe/tissue contact force being controlled by the scan assistant, as covered in Sec. III. To do this, the third frame, $\{S\}$, is defined as a moving frame that is constrained to follow the 3D surface of the breast, with the axes of $\{S\}$ corresponding to the normal and tangential vectors of the surface. The moving frame tracks the motion of the ultrasound probe as it is manually moved and will be used to define the desired orientation of the ultrasound probe. The desired 6-DoF position and orientation of the ultrasound probe are given by the vector ${}^{B}\vec{P}_d = [x_d, y_d, z_d, \alpha_d, \beta_d, \gamma_d]^\top$, where the x_d, y_d, and z_d components are the origin of the frame $\{S\}$. Given the ${}^{B}x$-${}^{B}y$ position of the ultrasound probe as it is moved, the origin of frame $\{S\}$ is given as

$$\begin{bmatrix} x_d \\ y_d \\ z_d \end{bmatrix} = \begin{bmatrix} {}^{B}x \\ {}^{B}y \\ {}^{B}z_c \end{bmatrix}, \tag{1}$$

such that the desired probe position (and origin of the frame) are constrained to the 3D surface.

The orientation of $\{S\}$ will be found through using the normal vector of the surface, ${}^{B}\vec{n}_c(x_d, y_d, z_d)$, where the partial derivative vectors

$$\begin{aligned} {}^{B}\vec{c}_{dx}(x_d, y_d, z_d) &= \left[1, 0, \frac{\partial f_c({}^{B}x, {}^{B}y)}{\partial x}\right]^\top \\ {}^{B}\vec{c}_{dy}(x_d, y_d, z_d) &= \left[0, 1, \frac{\partial f_c({}^{B}x, {}^{B}y)}{\partial y}\right]^\top, \end{aligned} \tag{2}$$

allow for the calculation of the normal vector

$${}^{B}\vec{n}_c(x_d, y_d, z_d) = \frac{{}^{B}\vec{c}_{dx}(x_d, y_d, z_d) \times {}^{B}\vec{c}_{dy}(x_d, y_d, z_d)}{\| {}^{B}\vec{c}_{dx}(x_d, y_d, z_d) \times {}^{B}\vec{c}_{dy}(x_d, y_d, z_d) \|} \tag{3}$$

using the cross product. During ultrasound scanning, to maintain adequate surface contact, the ultrasound probe needs to push downward on tissue parallel to the normal vector. Thus, the unit vector along the ${}^{S}z$, ${}^{S}\vec{n}_z = [0, 0, 1]$, will point into tissue along the normal vector of the surface. Utilizing the ${}^{B}z$ unit normal vector and a rotational transformation, the normal vector can be found. The normal vector ${}^{B}\vec{n}_c(x_d, y_d, z_d)$ is defined to be

$$\begin{aligned} -{}^{B}\vec{n}_c(x_d, y_d, z_d) &= {}^{B}_{S}R(\alpha_d, \beta_d, \gamma_d)\,{}^{S}\vec{n}_z \\ &= R_z(\gamma_d) \cdot R_y(\beta_d) \cdot R_x(\alpha_d) \cdot {}^{S}\vec{n}_z \\ = \begin{bmatrix} \cos\gamma_d & -\sin\gamma_d & 0 \\ \sin\gamma_d & \cos\gamma_d & 0 \\ 0 & 0 & 1 \end{bmatrix} &\cdot \begin{bmatrix} \cos\beta_d & 0 & \sin\beta_d \\ 0 & 1 & 0 \\ -\sin\beta_d & 0 & \cos\beta_d \end{bmatrix} \cdot \\ \begin{bmatrix} 1 & 0 & 0 \\ 0 & \cos\alpha_d & -\sin\alpha_d \\ 0 & \sin\alpha_d & \cos\alpha_d \end{bmatrix} &\cdot \begin{bmatrix} 0 \\ 0 \\ 1 \end{bmatrix}, \end{aligned} \tag{4}$$

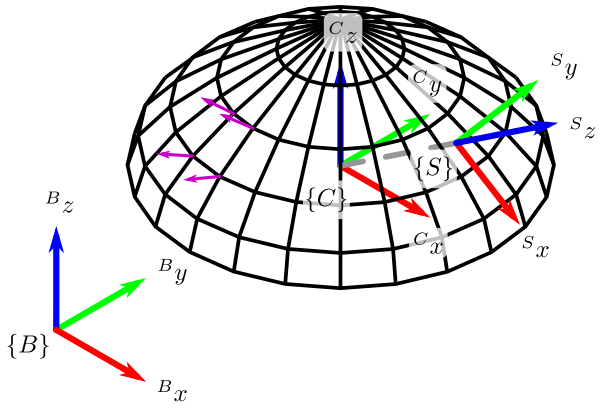

Fig. 1. Setup of frames for semi-autonomous breast scanning system, showing the robot base frame $\{B\}$, breast contour frame $\{C\}$, and moving surface frame $\{S\}$.

where the negative sign points the $^S z$ into the tissue and the multiplication of $R_x(\alpha_d)$, $R_y(\beta_d)$, and $R_z(\gamma_d)$ forms the rotation matrix $^B_S R(\alpha_d, \beta_d, \gamma_d)$. As the surface is defined within the $^B x - ^B y$ plane, the value of γ_d is a free parameter and is chosen to be zero ($\gamma_d \equiv 0$) which allows (4) to be simplified to

$$-{}^B\vec{n}_c(x_d, y_d, z_d) = \begin{bmatrix} \cos\alpha_d \sin\beta_d \\ -\sin(\alpha_d) \\ \cos\alpha_d \cos\beta_d \end{bmatrix} \tag{5}$$

which leads to the solutions[1]

$$\alpha_d = \text{asin}(-{}^B n_y) \tag{6}$$

and

$$\beta_d = \text{atan2}({}^B n_x, {}^B n_z), \tag{7}$$

with $^B n_x$, $^B n_y$, and $^B n_z$ representing the components of $^B\vec{n}_c(x_d, y_d, z_d)$. Thus, the desired position and orientation of the ultrasound probe can be found for any $^B x - ^B y$ point in the robot's workspace. Note that during the experiments, the calculation of partial derivatives and normal vectors were numerically approximated.

III. ROBOT MANIPULATOR CONTROL

Our robot controller is designed with two objectives in mind. First, the robot must be compliant to a user's physical input, i.e., pushing or pulling on the end-effector. Second, as the user moves the robot the position of the robot's tooltip should be controlled to be on the surface of the tissue and the robot's tooltip orientation should match the surface normal at the tooltip position.

[1]The solution to β_d is found by noting that

$$\frac{^B n_x}{^B n_z} = \frac{\cos\alpha_d \sin\beta_d}{\cos\alpha_d \cos\beta_d} = \tan(\beta_b)$$

A. Admittance Control for PHRI

As mentioned, an admittance controller is used to make the robot compliant and allow the user to adjust the position and orientation of the ultrasound probe. The transfer function of an admittance controller that specifies the desired velocity is given as

$$G = \frac{\vec{V}_d(s)}{\vec{W}(s)} = \frac{1}{Ms + B} \tag{8}$$

where the input to the controller, $\vec{W}(s) = \left[\vec{F}(s), \vec{\tau}(s)\right]^\intercal$, represents the wrench composed of input forces and torques, and the output, $\vec{V}_d(s)$, is the resulting desired velocity, composed of Cartesian and angular terms. M represents the desired mass and inertia matrix assigned to the robot and B represents the desired Cartesian and angular damping matrix. A stiffness parameter is not used as in [19] because restoring forces are not desirable during co-manipulation in free-space. Using the calculated desired velocity in conjunction with a velocity controller, we bypass the need for the robot's dynamics parameters while enabling adequately responsive force control of the robot.

To ensure the robot is compliant to user input (our controller's first objective), the user's interaction forces and torques are measured by a wrist-mounted force-torque sensor and provided as input to an admittance controller. The sensor readings are transformed to the robot frame:

$$^B\vec{W}_{Sensor} = {}^B_F T\, {}^F\vec{W}_{Sensor}$$

where $\vec{W}_{Sensor}$ represents the wrench read by the sensor and $^B_F T$ is the transformation matrix from the sensor frame to the robot base frame.

The admittance controller should allow the user to easily slide the robot along the surface of the tissue (i.e., moving in the $^S x - ^S y$ plane) while making it difficult for the user to move the probe in the direction normal to the tissue (i.e., along the $^S z$-axis). The interaction force along the $^S z$-axis should be handled by the robot itself in order to minimize deformation and maximize image quality on a repeatable basis. Similarly, the user should be able to slightly rotate the robot about the horizontal axes, $^B x$ and $^B y$, of the robot base frame to allow for adjustments to the probe's imaging angle. For these experiments, rotation about the vertical axis, $^B z$, is restricted to simplify the number of parameters the user was responsible for thereby improving repeatability. Thus, the user's force input should be transformed into frame $\{S\}$, while leaving the torque values unchanged (such that rotations initiated by the user are still made in frame $\{B\}$). We apply this transformation to Eq. (8) as follows:

$$\begin{aligned} ^B\vec{V}_{d,User} &= G_{User}\, ^B\vec{W}_{Sensor} \\ ^B\vec{V}'_{d,User} &= G'_{User}\, ^B\vec{W}'_{Sensor} \\ ^S_B T'\, ^B\vec{V}_{d,User} &= G'_{User}\, ^S_B T'\, ^B\vec{W}_{Sensor} \\ ^B\vec{V}_{d,User} &= {}^S_B T'^{-1} G'_{User}\, ^S_B T'\, ^B\vec{W}_{Sensor} \end{aligned} \tag{9}$$

where $^B\vec{V}_{d,User}$ and G_{User} represent the output velocity and admittance matrix associated with the user's input in

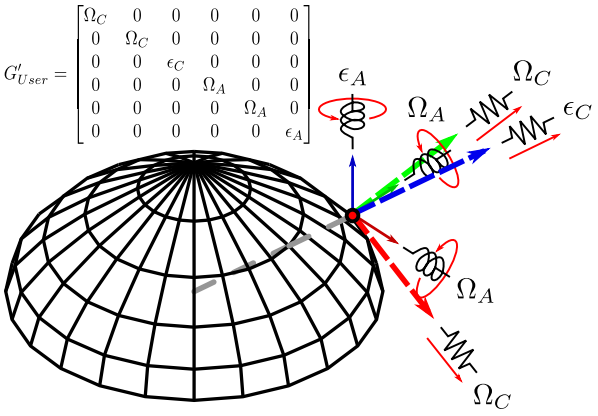

Fig. 2. Visualization of the admittance controller design. Virtual admittances control the ease with which the user can alter the ultrasound probe position (relative to the surface frame $\{S\}$) and orientation (relative to the base frame $\{B\}$).

the robot base frame. The variables with apostrophes represent their transformed versions with only the Cartesian components (i.e., forces) transformed to the frame $\{S\}$. ${}^S_B T'$ represents the transformation matrix which performs this rotation for only the Cartesian components. The transformed admittance matrix ${}^S_B T'^{-1} G'_{User} {}^S_B T'$ then provides the desired surface interaction, if G'_{User} is defined as

$$G'_{User} = \begin{bmatrix} \Omega_C & 0 & 0 & 0 & 0 & 0 \\ 0 & \Omega_C & 0 & 0 & 0 & 0 \\ 0 & 0 & \epsilon_C & 0 & 0 & 0 \\ 0 & 0 & 0 & \Omega_A & 0 & 0 \\ 0 & 0 & 0 & 0 & \Omega_A & 0 \\ 0 & 0 & 0 & 0 & 0 & \epsilon_A \end{bmatrix}$$

The admittance parameters in the surface's tangential directions (i.e., ${}^S x$ and ${}^S y$), Ω_C, and for rotation about the robot base frame's horizontal axes (i.e., ${}^B x$ and ${}^B y$), Ω_A, are large values. On the other hand, the admittance parameters in the surface's normal direction (i.e., ${}^S z$), ϵ_C, and for rotation about the robot base frame's vertical axis (i.e., ${}^B z$), ϵ_A, are small values[2]. Fig. 2 provides a visualization of the transformed admittances in G'_{User}.

B. Pose Tracking for Optimal Imaging

To ensure the probe is in contact with the tissue surface and that its orientation is optimal (i.e., normal to the tissue surface), a position error-based input to the velocity controller is used to bring the robot to a desired pose, in relation to its position in the ${}^B x$ and ${}^B y$ axes as mentioned in Section II. A lookup is performed on the reference surface data, providing the desired pose for the robot-end-effector to track, ${}^B\vec{P}_{Surface} = \left[{}^B x,\ {}^B y,\ {}^B z,\ {}^B \alpha,\ {}^B \beta,\ {}^B \gamma \right]^\intercal$. We then define an error term between the desired pose and the robot's current pose as

$$e = {}^B\vec{P}_{Surface} - {}^B\vec{P}_{Probe}$$

In order to minimize the error over a period of time, the velocity commanded to the robot, ${}^B\vec{V}_{d,Pose}$, can be used as given:

$$e = {}^B\vec{P}_{Surface} - \int_{t_0}^{t} {}^B\vec{V}_{d,Pose} dt - {}^B\vec{P}_{Probe} \tag{10}$$

Rearranging Eq. (10), we then generate a proportional desired velocity as input into the velocity controller by equating the error to zero:

$$\begin{aligned} {}^B\vec{V}_{d,Pose} &= \frac{{}^B\vec{P}_{Surface} - {}^B\vec{P}_{Probe}}{t - t_0} \\ &= K \left({}^B\vec{P}_{Surface} - {}^B\vec{P}_{Probe} \right) \end{aligned} \tag{11}$$

Here, K is a matrix of gains[3] that describe the desired duration of movement needed to match the desired position, given as

$$K = \begin{bmatrix} k_x & 0 & 0 & 0 & 0 & 0 \\ 0 & k_y & 0 & 0 & 0 & 0 \\ 0 & 0 & k_z & 0 & 0 & 0 \\ 0 & 0 & 0 & k_\alpha & 0 & 0 \\ 0 & 0 & 0 & 0 & k_\beta & 0 \\ 0 & 0 & 0 & 0 & 0 & k_\gamma \end{bmatrix}$$

Finally, the command velocity for the robot's velocity controller is given through the combination of Eq. (9) and (11):

$${}^B\vec{V}_d = {}^B\vec{V}_{d,User} + {}^B\vec{V}_{d,Pose} \tag{12}$$

A block diagram of the control loop incorporating both the human-in-the-loop and autonomous elements is presented in Fig. 3.

IV. EXPERIMENTAL SETUP AND RESULTS

During the experiments, the robotic assistance system will be used to aid a user in a simulated pre-planning breast brachytherapy scanning procedure. The ultrasound transducer, see Fig. 4, was connected to a Gamma-Net force/torque sensor (ATI Industrial Automation, Apex, NC, USA) and was mounted on a Motoman SAI-5F robot (Yaskawa America Inc, Miamisburg, OH, USA). The ultrasound machine used for the experiments was an Ultrasonix Touch with a 4DL14-5/38 Linear 4D transducer (Ultrasonix Corp, Richmond, BC, Canada). For these experiments, only the 2D imaging functionality of the ultrasound probe was used. The image processing and admittance controller were programmed and implemented in Matlab 2017a (The Mathworks Inc, Natwick, MA, USA) and ran using the Simulink Real-Time environment, on an Intel Core i7-3930K running at 3.20 GHz (Intel Corporation, Santa Clara, CA, USA). A phantom tissue sample of a breast with an underlying seroma is used as the imaging target. The phantom tissue is created by placing a water-filled pocket inside a plastisol phantom (M-F Manufacturing Co, Fort Worth, USA).

[2]Experimental values of the admittance parameters as described in Eq. (8) were selected as $(M,B)_{\Omega_C} = (0.01\frac{Ns^2}{mm}, 0.5\frac{Ns}{mm})$, $(M,B)_{\epsilon_C} = (0.03\frac{Ns^2}{mm}, 1.5\frac{Ns}{mm})$, $(M,B)_{\Omega_A} = (0.1\frac{Ns^2}{rad}, 1\frac{Ns}{rad})$, and $(M,B)_{\epsilon_A} = (1.5\frac{Ns^2}{rad}, 15\frac{Ns}{rad})$.

[3]Experimental values of the position error gains were selected as $k_x = k_y = k_z = k_\alpha = k_\beta = k_\gamma = 0.5s^{-1}$ through trial and error.

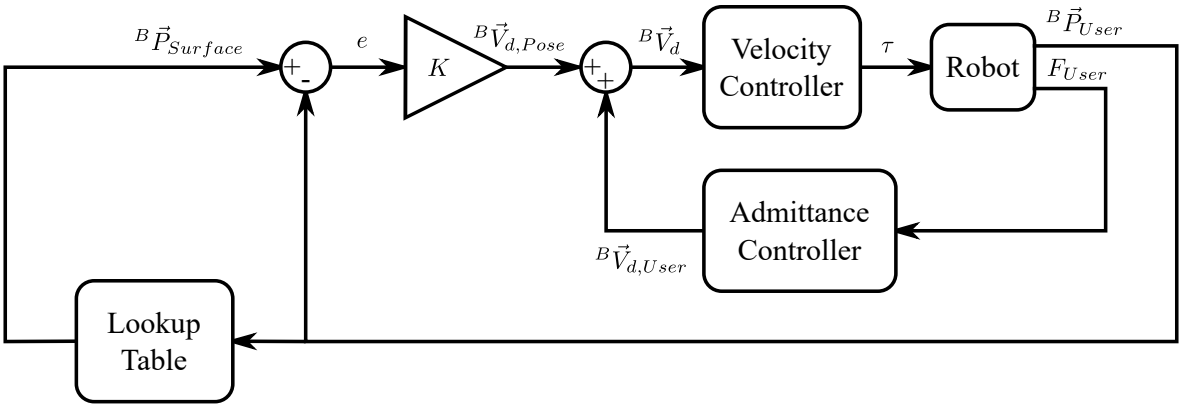

Fig. 3. Admittance controller loop.

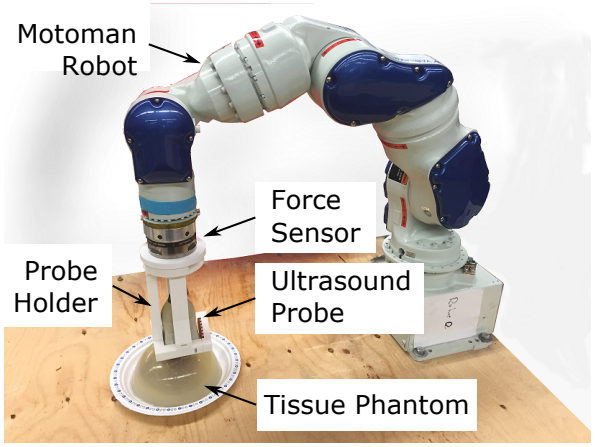

Fig. 4. Experimental setup including 7-DoF robot, ultrasound probe, force sensor, and tissue phantom.

The robotic ultrasound scanning assistant is designed to assist clinicians and medical imaging personnel through ensuring proper ultrasound/tissue contact and transducer orientation so that high-quality ultrasound scans of breast tissue can be performed with minimal manual effort. To evaluate this, a proof-of-concept study was performed to measure imaging quality achieved when a lay user is assisted with an ultrasound scan by the system.

A set of "ideal" ground-truth ultrasound images $^G I_{US}(px, py)$ of the breast phantom were captured before the user trials. To capture these images, the 7-DoF robotic system was programmed to scan the tissue phantom with a constant US probe contact force in a fully-autonomous position-controlled manner. The fully autonomous scan thus contains images captured as if the semi-autonomous controller had both "ideal" force and position tracking performances. Each of the ground-truth images shows a $^B x - {}^B z$ planar slice of the breast phantom, with each image taken on an evenly spaced 5 mm grid (in the $^B x - {}^B y$ plane) over the entire tissue phantom. For the fully autonomous scan and the user trials, a target contact force of 3 N was used as this force was empirically found to offer acceptable image quality with minimal tissue deformation.

TABLE I

USER TRIAL IMAGE QUALITY COMPARISON RESULTS

User Trial	Average SSD Score	Min SSD Score	Max SSD Score
1	6.65(±1.10)	4.99	8.08
2	7.55(±0.49)	5.86	7.95
3	7.56(±0.32)	6.75	8.01
4	7.11(±0.92)	5.59	8.24
5	6.99(±0.40)	6.02	7.56
6	6.70(±0.96)	4.40	7.98
7	7.19(±0.75)	5.52	8.03
8	6.79(±1.09)	4.73	8.15
9	6.21(±0.84)	4.71	7.45
10	6.75(±0.75)	4.62	7.73

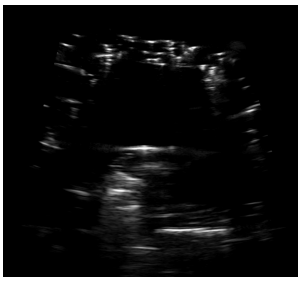

(a) US image captured during user trial.

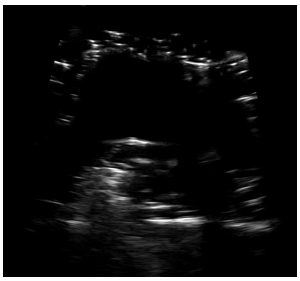

(b) Nearest ground truth image .

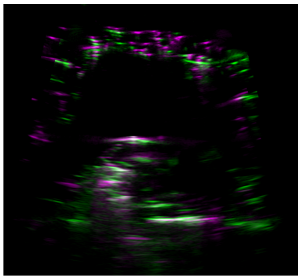

(c) Registration of the images in Fig. 5(a) and Fig. 5(b)

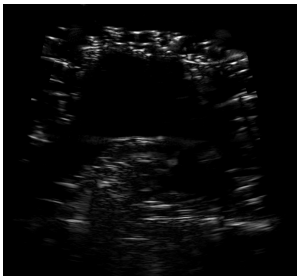

(d) Normalized cross-correlation between the images in Fig. 5(a) and Fig. 5(b) after registration.

Fig. 5. US image registration and SSD measurement.

For the user trials, the probe held by the robotic assistant was placed at a predefined starting point on the breast phantom. The user was asked to scan from one side of the tissue phantom to the other three times in a forward-backward-forward pattern. Ultrasound images, denoted by ${}^{U}I_{US}(px, py)$ (in the ultrasound frame $\{U\}$), were captured by the system as the user scanned over the phantom. These images are then compared to the to the nearest ground-truth image ${}^{G}I_{US}(px, py)$ from the fully autonomous scan. The image quality of the semi-autonomous controller was measured by evaluating the sum of squared differences (SSD) [20] between the user and ground truth images; see Figures 5(a), 5(b), and 5(d).

Rigid registration was used to align the user trial and ground truth images for SSD calculation, thus removing any rotational and translational offset between them. This registration step is required because the user is free to move the ultrasound probe as they wish during the scan and therefore the position at which a semi-autonomous trial image is captured wasn't constrained to correspond to the ground-truth image locations. While in general non-rigid registration would be required for US-image to US-image registration [21], this would have removed any scaling differences between the two image sets caused by suboptimal probe orientation control.

For registration, minimum eigenvalue feature points common to each of the two images were found and the transform ${}^{G}P = {}^{G}_{U}T\,{}^{u}P$ between these matched points in the two images was calculated, as shown in Fig. 5(c). The transform performs rigid registration between the two images, given by

$$ {}^{G}_{U}T = \begin{bmatrix} \cos {}^{G}_{U}\phi & -\sin {}^{G}_{U}\phi & {}^{G}_{U}t_x \\ \sin {}^{G}_{U}\phi & \cos {}^{G}_{U}\phi & {}^{G}_{U}t_y \\ 0 & 0 & 1 \end{bmatrix} \tag{13} $$

where ${}^{G}_{U}\phi$ is the angular offset between the two images and ${}^{G}_{U}t_x$ and ${}^{G}_{U}t_y$ are the x and y transitional offsets between the two frames.

As the user was allowed to scan the phantom as they wished, the scanning time for each user trial is different. To compensate for this in the results shown in Table I, a set of 100 evenly spaced (across the total time of the scan) images from each user trial were compared to the nearest ground-truth images. The mean of the image based SSD value (between the user and ground-truth images) was used to score how closely the two images match and give a measure of image quality. A semi-autonomous trial US image which exactly matches the ground-truth fully autonomous image will have an SSD score of 0 and a noisy or low-quality image will have a large SSD value. As an example, when poor contact is made between the probe and tissue, the high acoustic impedance mismatch between the probe and air will cause the output image to be substantially distorted [22], resulting in a high SSD score (greater than 30). The results in Table I show that the system achieves image quality similar to a fully-autonomous scan, at the chosen force value, for semi-autonomous control with a lay user operator.

V. Conclusions

A semi-autonomous ultrasound scanning robotic assistant was presented in this work with the goal of minimizing tissue deformation and increasing imaging repeatability. Control of probe/tissue contact and the angle of the probe on the tissue surface was performed autonomously, while positioning of the probe along the surface of the breast was controlled by the human operator through the use of an admittance controller. A feasibility study was performed to evaluate imaging quality. Scans of a phantom tissue with a simulated seroma were performed with two sets of trials, one involving a human-in-the-loop and the other with fully-autonomous robot control. Image registration between the obtained ultrasound images of the two image sets showed that the system achieved reasonable image quality while allowing the user to freely scan the tissue.

Future work will involve user trials to find a balance between probe control performance, image quality, and a subjective ease-of-use metric for the system. Several improvements to the system are also desired. First, a snap-to-grid modality will be highly beneficial for increasing imaging repeatability, where the robot moves to the nearest point on a grid of attractor points overlaid on the tissue. A stability analysis of this system will also have to be performed. Implementation of an impedance controller as opposed to an admittance controller will also be beneficial for improving interactions with human tissue and for PHRI. Alternatively, a mechanically backdriveable, lightweight and patient-safe robot can be used. Optimizing the pose of the robot and the design of the probe attachment will also be investigated in order to maximize the workspace available.

References

[1] Canadian Cancer Societys Advisory Committee on Cancer Statistics, "Canadian cancer statistics 2017," Canadian Cancer Society, Toronto, ON, Tech. Rep., 2017.

[2] A. N. Sencha, E. V. Evseeva, M. S. Mogutov, and Y. N. Patrunov, *Breast Ultrasound*. Springer-Verlag Berlin Heidelberg, 2013.

[3] C. Rossa and M. Tavakoli, "Issues in closed-loop needle steering," *Control Engineering Practice*, vol. 62, pp. 55 – 69, 2017.

[4] J. Michael, D. Morton, D. Batchelar, M. Hilts, J. Crook, and A. Fenster, "Development of a 3D ultrasound guidance system for permanent breast seed implantation," *Medical Physics*, vol. 45, no. 8, pp. 3481–3495, 2018.

[5] M. Zanotel, I. Bednarova, V. Londero, A. Linda, M. Lorenzon, R. Girometti, and C. Zuiani, "Automated breast ultrasound: basic principles and emerging clinical applications," *La radiologia medica*, vol. 123, no. 1, pp. 1–12, Jan 2018.

[6] Siemens Healthcare GmbH, "ACUSON S2000 ABVS Ultrasound System, HELX Evolution with Touch Control." [Online]. Available: https://www.healthcare.siemens.com/ultrasound/breast-care/acuson-s2000-abvs-ultrasound-machine

[7] J. Carriere, M. Khadem, C. Rossa, N. Usmani, R. Sloboda, and M. Tavakoli, "Event-triggered 3d needle control using a reduced-order computationally efficient bicycle model in a constrained optimization framework," *Journal of Medical Robotics Research*, vol. 0, no. 0, p. 1842004, Accepted.

[8] ——, "Surgeon-in-the-loop 3-d needle steering through ultrasound-guided feedback control," *IEEE Robotics and Automation Letters*, vol. 3, no. 1, pp. 469–476, Jan 2018.

[9] B. Fallahi, C. Rossa, R. S. Sloboda, N. Usmani, and M. Tavakoli, "Sliding-based image-guided 3d needle steering in soft tissue," *Control Engineering Practice*, vol. 63, pp. 34 – 43, 2017.

[10] M. Khadem, C. Rossa, N. Usmani, R. S. Sloboda, and M. Tavakoli, "Semi-automated needle steering in biological tissue using an ultrasound-based deflection predictor," *Annals of Biomedical Engineering*, vol. 45, no. 4, pp. 924–938, Apr 2017.

[11] J.-P. Pignol, J.-M. Caudrelier, J. Crook, C. McCann, P. Truong, and H. A. Verkooijen, "Report on the clinical outcomes of permanent breast seed implant for early-stage breastcancers," *International Journal of Radiation Oncology*Biology*Physics*, vol. 93, no. 3, pp. 614 – 621, 2015.

[12] N. Hogan and S. P. Buerger, "Impedance and interaction control," in *Robotics and automation handbook*, T. R. Kurfess, Ed. CRC press, 2004, ch. 19.

[13] G. Zeng and A. Hemami, "An overview of robot force control," *Robotica*, vol. 15, no. 5, pp. 473–482, 1997.

[14] W. S. Newman, "Stability and performance limits of interaction controllers," *Journal of Dynamic Systems, Measurement, and Control*, vol. 114, no. 4, p. 563, 1992.

[15] J. Fong and M. Tavakoli, "Kinesthetic teaching of a therapist's behavior to a rehabilitation robot," in *2018 International Symposium on Medical Robotics (ISMR)*, March 2018, pp. 1–6.

[16] E. T. Wolbrecht, V. Chan, D. J. Reinkensmeyer, and J. E. Bobrow, "Optimizing compliant, model-based robotic assistance to promote neurorehabilitation," *IEEE Transactions on Neural Systems and Rehabilitation Engineering*, vol. 16, no. 3, pp. 286–297, 2008.

[17] M. Mitsuishi, S. Warisawa, T. Tsuda, T. Higuchi, N. Koizumi, H. Hashizume, and K. Fujiwara, "Remote ultrasound diagnostic system," in *Proceedings 2001 ICRA. IEEE International Conference on Robotics and Automation (Cat. No.01CH37164)*, vol. 2, May 2001, pp. 1567–1574 vol.2.

[18] F. Conti, J. Park, and O. Khatib, "Interface design and control strategies for a robot assisted ultrasonic examination system," in *Experimental Robotics*. Springer, 2014, pp. 97–113.

[19] F. Dimeas and N. Aspragathos, "Online stability in human-robot cooperation with admittance control," *IEEE Transactions on Haptics*, vol. 9, no. 2, pp. 267–278, April 2016.

[20] R. C. Gonzalez and R. E. Woods, *Digital image processing*. Upper Saddle River, N.J. : Prentice Hall, 2002.

[21] C. Che, T. S. Mathai, and J. Galeotti, "Ultrasound registration: A review," *Methods*, vol. 115, pp. 128 – 143, 2017, image Processing for Biologists.

[22] H. Azhari, *Basics of Biomedical Ultrasound for Engineers*. Wiley-IEEE Press, 2010.